

Recurrent Neural Network Control of a Hybrid Dynamic Transfemoral Prosthesis with EdgeDRNN Accelerator

Chang Gao^{*,1}, Rachel Gehlhar^{*,2}, Aaron D. Ames², Shih-Chii Liu¹ and Tobi Delbruck¹

Abstract—Lower leg prostheses could improve the lives of amputees by increasing comfort and reducing energy to locomote, but currently the control methods make it difficult to modulate behaviors based upon the human’s experience. This paper describes the first steps toward learning complex controllers for dynamic robotic assistive devices. We provide the first example of behavioral cloning to control a powered transfemoral knee and ankle prostheses using a Gated Recurrent Unit (GRU) based recurrent neural network (RNN) running on a custom hardware accelerator that exploits temporal sparsity. The RNN is trained on data collected from the original prosthesis controller. The RNN inference is realized by a novel EdgeDRNN accelerator in real-time. Experimental results show that the RNN can model the dynamic system with impacts and replace the nominal PD controller to realize end-to-end control of the AMPRO3 prosthetic leg walking on flat ground and unforeseen slopes with comparable tracking accuracy. EdgeRNN computes the RNN about 240 times faster than real time, opening the possibility of more complex future optimizations. Implementing an RNN on this real-time dynamic system with impacts sets the ground work to incorporate other learned elements of the human-prosthesis system into prosthesis control.

I. INTRODUCTION

Even though there are over 222,000 transfemoral amputees in the United States [1], the market for prostheses remains largely limited to passive devices. These prostheses limit amputees’ daily life by increasing their metabolic cost and constricting their locomotion abilities [2]. Transfemoral amputees expend around 30% more energy in walking compared to healthy humans [3]. Powered prostheses can reduce this metabolic cost and also increase their comfortable walking speed by providing net power to the user [4], [5]. This power is also particularly helpful for high energy tasks like stair-climbing [6], [7]. Motivated by this need, research on powered leg prostheses has largely focused on impedance control [6], [8]–[10]. Impedance control models each joint as

*This work was supported by the Samsung Global Research *Neuromorphic Processor Project* and the National Science Foundation Graduate Research Fellowship under Grant No. DGE1745301 and NSF NRI Grant No. 1724464. This research was approved by California Institute of Technology Institutional Review Board with protocol no. 16-0693 for human subject testing. The authors also gratefully acknowledge discussions with Andrew Taylor and Prof. Yisong Yue, and the opportunity to build the first prototype at the July 2019 Telluride Neuromorphic Engineering Workshop.

^{*}The authors contributed equally to this work.

¹Chang Gao, Shih-Chii Liu, Tobi Delbruck are with the Institute of Neuroinformatics, University of Zurich and ETH Zurich, Winterthurerstrasse 190, Switzerland chang@ini.uzh.ch, shih@ini.uzh.ch, tobi@ini.uzh.ch

²Rachel Gehlhar and Aaron D. Ames are with the Department of Mechanical and Civil Engineering, California Institute of Technology, 1200 East California Boulevard, Pasadena, CA 91125, USA rgehlhar@caltech.edu, ames@caltech.edu

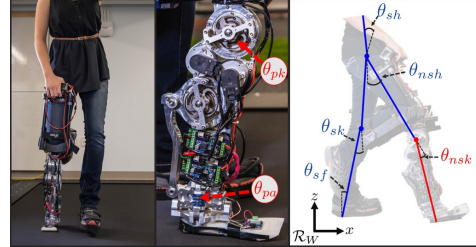


Fig. 1: (Right) Human subject walking on powered transfemoral prosthesis, AMPRO3 (Middle). (Left) Robot model of human-prosthesis system labeled with joint angles.

a spring-damper system where the spring constant, damping coefficient, and equilibrium are parameters tuned by the user. Hence impedance control requires extensive tuning and is largely heuristic. To address this limitation, [11] developed a trajectory generation method for powered prostheses that can be tracked by various online controllers, such as PD control. The controller drives the motors’ actual joint angles to the desired joint trajectories to yield human-like walking of the human prosthesis system. However, the PD controller is very limited in its knowledge of the human-prosthesis system and hence its ability to control the prosthesis in response to the human.

To address the drawbacks of existing control methods, we investigate RNNs which have been used to understand human motion and to produce an input for prosthetic control systems. [12] uses RNNs to predict joint angles of human lower limbs based on surface electromy signals, for future application to lower-limb rehabilitation robotics. Similarly [13] used RNNs to model the relation between arm muscles to finger flexion using surface myoelectric sensors and flexion sensors. Here, the RNNs outputs are used as reference signals for a PID controller to control a prosthetic hand. For lower-limb control, [14] used an RNN to estimate gait phase from an inertial measurement unit (IMU) for a powered ankle exoskeleton. This research used RNNs to model physical dynamics but none used RNNs for direct control of prostheses, which we realize in this paper using imitation learning.

Imitation learning has been used to reproduce human gestures on robots using hidden Markov model and Gaussian mixture regression [15]. [16] used a feed-forward deep neural network for online trajectory optimization with Model-Predictive Control (MPC) in a continuous dynamic system. Imitation learning with high level motion primitives in non-agile hybrid systems such as vision-based planning and control are popular, including [17], [18]. To the best of

our knowledge, no research combines RNNs with imitation learning in a dynamic hybrid system with impacts. While control by an RNN can result in unprovable stability, the potential advantages to having an RNN capable of performing real-time control on a prosthesis includes both building simpler models of complex controllers and dynamics for efficient computing, and capturing the nonlinearities and complexities of human walking behavior to include in prosthesis control methods.

In this study, we replaced the conventional PD controller with a gated-recurrent unit (GRU) RNN [19] using imitation learning. The RNN is trained on data collected during PD control of AMPRO3 walking on flat ground. An energy-efficient entry-level field programmable gate array (FPGA) accelerator called EdgeDRNN is used to run the RNN in real time. Experimental results show equivalent functionality between the RNN controller and the PD controller walking on flat ground and even on unseen slopes. These results are demonstrated by experimental joint trajectory and torque data and by the supporting video¹. The main contributions of this paper are:

- 1) First instance of imitation learning for hybrid dynamic systems with impacts;
- 2) First realization of an end-to-end RNN control of a robotic prosthesis functioning with a human in the real-world using behavioral cloning;
- 3) First work to use a hardware-accelerated RNN for real-time control.

By proving this RNN's ability to work on this dynamic system with impacts, we establish the first steps in using an RNN to improve upon existing prosthesis control methods. By learning other aspects of the human-prosthesis system, such as human comfort preferences [20], various gait styles, and motion intent for transitions, we can bring the human into the loop of prosthesis control.

II. BACKGROUND

This section introduces the framework of the traditional process of prosthesis controller generation that will be leveraged in the learning process, which is outlined subsequently.

A. AMPRO with PD Controller

We first present an overview of the methodology for synthesizing PD controllers for powered prostheses - specifically, AMPRO3 (Fig. 1), a powered transfemoral prosthesis developed at Caltech [21]. In particular, this prosthesis with an actuated knee and ankle joint is modeled as a hybrid dynamical system. Desired outputs are defined that guide the behavior of the prosthesis wherein the parameters of these outputs are determined by an optimization problem that enforces impact invariance of these outputs [22]. The end results are desired trajectories that are tracked via PD control on the device.

Human-Prosthesis Model and Outputs. Trajectories are designed for the whole human-prosthesis system to yield

stable walking. The system is modeled as a 5-link planar bipedal robot with configuration space $\mathcal{Q}_R : \theta = (\theta_{sf}, \theta_{sk}, \theta_{sh}, \theta_{nsh}, \theta_{nsk})$, as shown in Fig. 1 [23].

To yield human-like walking, the control goal is to drive the actual robot outputs $y^a(\theta, \dot{\theta})$ to desired human outputs $y^d(t, \alpha)$. These desired trajectories $y_2^d(t, \alpha)$ are defined by the canonical walking function with a parameter set α :

$$y_2^d(t, \alpha) = e^{-\alpha_4 t} (\alpha_1 \cos(\alpha_2 t) + \alpha_3 \sin(\alpha_2 t)) + \alpha_5.$$

To develop a more robust controller, the trajectories are parameterized with a state-based phase variable:

$$\rho(\theta) = \frac{\delta p_{hip}(\theta) - \delta p_{hip}^+}{v_{hip}}$$

in place of t in the desired trajectories: $y_2^d(\rho(\theta), \alpha)$, where $\delta p_{hip}(\theta)$ is the linearized forward hip position, which increases linearly in a step cycle [24]. Five outputs are defined for the robot model: forward hip velocity (*hip*), knee angles (*sk*, *nsk*), non-stance slope (*nsl*), and torso angle (*tor*). For details, see [25]. The human-inspired outputs [22] are defined as:

$$y(\theta, \dot{\theta}, \alpha) = \begin{bmatrix} y_1(\theta, \dot{\theta}, \alpha) \\ y_2(\theta, \alpha) \end{bmatrix} = \begin{bmatrix} y_1^a(\theta, \dot{\theta}) - v_{hip} \\ y_2^a(\theta) - y_2^d(\rho(\theta), \alpha) \end{bmatrix}$$

where the relative degree one output $y_1(\theta, \dot{\theta}, \rho, \alpha)$ is the difference between the actual and desired hip velocity, and the relative two outputs $y_2^a(\theta) - y_2^d(\rho, \alpha)$ are the differences between the actual and desired positions listed above as the last 4 outputs.

Gait Generation. To obtain human-like walking trajectories for $y_2^d(\rho(\theta), \alpha)$, we first model the system as a hybrid system [22] to account for the discrete dynamics present at foot impact in walking. The impacts cause a discrete jump in the velocity of a walking robot model and could throw the system off of its desired trajectories. Hence, in our trajectory generation we enforce that the tracking of the relative degree 2 outputs remains invariant through impacts. These constraints, termed *partial hybrid zero dynamics* constraints [22], are included in our optimization to solve for the parameters α and v_{hip} , which define our desired trajectories. Details can be found in [26].

Prosthesis Control. To apply a PD controller for trajectory tracking, the desired prosthesis knee angle θ_{pk}^d is determined from the desired trajectory $y_{2,sk}^d(\rho(\theta), \alpha)$ for the prosthesis stance phase and $y_{2,nsk}^d(t, \alpha)$ for the prosthesis non-stance phase. State-based control is used for the prosthesis stance phase to respond to the human's speed of progression in walking and direction of progression, i.e. forward or backward. This domain ends when $\rho(\theta) = \rho_{max}$, a constant determined by the user through testing. Time-based control is used for prosthesis swing since the prosthesis does not have access to the human's stance hip position for the phase variable. Here t is used in $y_{2,nsk}^d(t, \alpha)$. This domain ends when $t = t_{max}$, a constant determined through optimization. For both phases θ_{pa}^d is set to 0 to act as a passive joint.

¹https://youtu.be/mzMSEo2S_hg

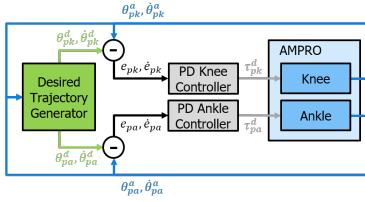


Fig. 2: Architecture of the AMPRO PD control system.

To have the actual prosthesis knee and ankle angles ($\theta_{pk}^a, \theta_{pa}^a$) track these desired positions and velocities, a PD controller calculates the desired torque $\tau_{j,k}^d$ as follows:

$$\tau_{j,k}^d = K_{j,v}^P (\theta_j^a - \theta_j^d) + K_{j,v}^D (\dot{\theta}_j^a - \dot{\theta}_j^d),$$

where $j \in \{pk, pa\}$ indicates the joint and $v \in \{pt, pw\}$ signifies the given phase the controller is acting in, where ps stands for *prosthesis stance* and pns for *prosthesis non-stance*. The PD gains ($K_{j,v}^P, K_{j,v}^D$ for $j \in \{pk, pa\}$) and $v \in \{pt, pw\}$ are selected such that the closed-loop linear output system is stable [22].

B. Recurrent Neural Networks

Recurrent neural networks (RNNs) are a family of artificial neural networks that are universal function approximators [27]. RNNs have recurrent connections between their outputs and inputs and are a popular method in machine learning to model time series. State-of-the-art RNNs like the Gated-Recurrent Unit (GRU) [19] and Long Short-Term Memory (LSTM) [28] models add gating units to the neurons. These units can overcome the vanishing gradient problem during training. These RNNs achieve high accuracy and are commercially deployed on many real-world tasks such as speech recognition and natural language processing. Outputs of a controller in a system can be seen as functions of sequential inputs; thus, RNNs are a candidate to approximate the temporal dependencies between outputs and inputs of the original controller.

Gated-Recurrent Unit & Delta Networks. In this work, a GRU-RNN based network is used to control AMPRO3. GRU-RNNs are computationally expensive and difficult to process on an embedded system in real time. Recurrent connections create data dependency between RNN inputs and outputs limiting the parallelism of this algorithm. Thus, the memory bandwidth is the bottleneck of RNN computation on an embedded system. Modern von Neumann architecture based processors, such as GPUs, suffer from low utilization rate of arithmetic units when running RNNs using a small batch size due to the insufficient memory bandwidth to external memory. Because of the poor power efficiency of GPUs on RNN inference with batch size of 1 of around 1.1 GOP/s/W [29], they are not suitable for a portable device with limited power budget like AMPRO3.

We proposed the bio-inspired DeltaGRU [30] as an RNN variant that reduces the operations required for computing GRU-RNNs. Instead of multiplying weights with input and hidden activations as in GRU-RNNs, in DeltaGRU weights are multiplied with the the change of activations between two adjacent time steps and then added to a memory term that

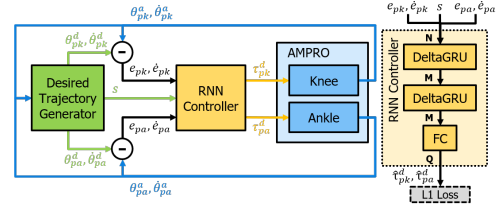


Fig. 3: Architecture of the proposed AMPRO3 RNN controller system and the network structure.

is the accumulation of all previous products. By skipping the elements of a delta vector when their individual values are less than a defined threshold, the number of the corresponding matrix-vector multiply-and-accumulate (MAC) operations can typically be reduced by about a factor of 10 without loss of accuracy [30].

EdgeDRNN Accelerator. The second generation DeltaRNN (DRNN) accelerator (based on [31]) used in this paper is called EdgeDRNN [32]. Like the original one, it skips unnecessary MAC operations by exploiting temporal sparsity like spiking neural networks, but it utilizes external DRAM memory for the large weight matrices. This way it reduces the latency of the RNN inference and enables cheaper real-time inference. EdgeDRNN has 8 MAC units that support 16-bit fixed-point activations and 8-bit fixed-point weights. With a 100 MHz clock frequency, EdgeRNN has a peak throughput of 3.2 GOp/s and with up to 118 GOp/s measured effective² throughput when running a large multi-layer DeltaGRU network, even with batch size 1, where weight reuse is not feasible.

III. CONTROLLER DESIGN

This section outlines how the RNN controller is constructed with training data from the AMPRO3 prosthesis.

A. RNN Controller

Figure 3 shows the AMPRO3 control system architecture where the two original PD controllers for the knee and ankle are now replaced by the RNN controller. An additional scalar input, s to the RNN controller is the swing status calculated by the Desired Trajectory Model indicating whether the human leg is in swing phase or not. The model on the right of the figure shows the 2 GRU layers and 1 fully-connected (FC) layer of the RNN controller. Each GRU layer has M neurons. The input dimension of the first GRU layer is $N = 5$. The FC layer has Q neurons to map the M -dimensional GRU-RNN output vector to a Q -dimensional vector, where $Q = 2$ is the number of regression target variables and also the output vector dimension of the whole network. The following steps are required to deploy the RNN on AMPRO3:

- 1) Collect data and labels from a demonstrator, which is the original PD controller. A user walks on AMPRO3

²1 MAC is 2 Op; *effective throughput* accounts for skipped operations from the delta operation.

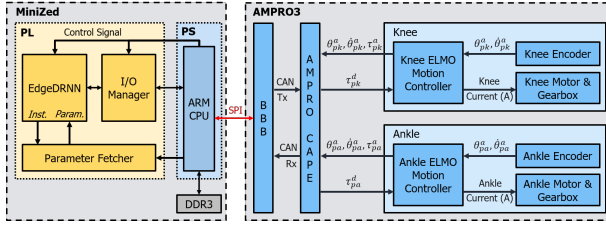


Fig. 4: Block diagram of the hardware system with MiniZed and AMPRO3.

for an amount of time while the inputs and outputs of the demonstrator are recorded simultaneously. The recorded data are divided into training, validation, and test sets.

- 2) Train the RNN controller network on the collected training set data and select network parameters using the validation set.
- 3) Evaluate the performance of the RNN controller on the test set.
- 4) Implement the RNN controller on the EdgeDRNN accelerator to control AMPRO3.

B. Data Collection & Processing

Data was collected by a subject walking with AMPRO3 on flat ground 5 times. Each walk takes around 70 seconds. All 5 walks give around 70,079 time steps of data in total with 200 Hz sample rate. Each sample contains the desired and actual positions of the knee ($\theta_{pk}^d, \theta_{pk}^a$) and ankle ($\theta_{pa}^d, \theta_{pa}^a$), desired and actual velocities of the knee ($\dot{\theta}_{pk}^d, \dot{\theta}_{pk}^a$) and ankle ($\dot{\theta}_{pa}^d, \dot{\theta}_{pa}^a$), phase flag s ($s = 0$ for prosthesis non-stance, $s = 1$ for prosthesis stance), and desired torques of the knee (τ_{pk}^d) and ankle (τ_{pa}^d). Errors between the desired and actual positions e_{pk}, e_{pa} and velocities $\dot{e}_{pk}, \dot{e}_{pa}$ are calculated using aforementioned data. Three out of the five data files are used as the training set while both the validation and the test set have 1 data file each. Since the data are time series, we set a sequence length of T time steps and stride of 1 time step to select sequences out of each set. Training labels are given by τ_{dk} and τ_{da} .

C. Training Procedure

The RNN controller network acts as a policy π with parameters λ that map inputs from the current and previous time steps to outputs of the current time, which is given as:

$$\begin{aligned} \mathbf{x}_t &= [e_{pk,t}, e_{pa,t}, \dot{e}_{pk,t}, \dot{e}_{pa,t}, s_t], \\ \hat{\mathbf{y}}_t &= [\hat{\tau}_{pk,t}^d, \hat{\tau}_{pa,t}^d], \\ \hat{\mathbf{y}}_t &= \pi_\lambda(\mathbf{x}_t, \hat{\mathbf{y}}_{t-1}), \end{aligned}$$

where \mathbf{x}_t and $\hat{\mathbf{y}}_t$ are the input and output vectors respectively at time step t . To train the network to infer the desired torques $\hat{\tau}_{pk,t}^d, \hat{\tau}_{pa,t}^d$ (i.e. a regression task), batches of training data are fed to the network for forward propagation. For each batch, the L1 loss is calculated as:

$$\begin{aligned} \ell_t^i(\mathbf{y}_t^i, \hat{\mathbf{y}}_t^i) &= |\mathbf{y}_t^i - \hat{\mathbf{y}}_t^i|, \\ \mathcal{L} &= \frac{1}{N \times T} \sum_{i=1}^N \sum_{t=1}^T \ell_t^i, \end{aligned}$$

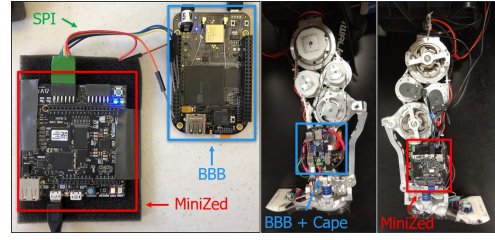


Fig. 5: The MiniZed is attached to AMPRO3 and connected to the BBB through an SPI interface.

where i is the index of a sequence in a batch, $\mathbf{y}_t^i = [\tau_{dk,t}^i, \tau_{da,t}^i]$ the vector of labels, ℓ_t^i the loss of time step t , \mathcal{L} the loss of a batch with sequences of length T . The L1 loss is used instead of the L2 loss because of its robustness to outliers [33].

IV. HARDWARE IMPLEMENTATION

The hardware of the original AMPRO3 and the EdgeRNN systems and their integration will be covered in this section.

A. AMPRO3

Figure 4 shows the control architecture, including sensing and computation, of AMPRO3 [21]. It is run on a Beagle-Bone Black (**BBB**) micro-controller on-board the prosthetic. The BBB controller is coded in C++ and runs in a Robot Operating System at 200 Hz. A custom printed circuit board called AMPRO Cape for the BBB includes a Controller Area Network (**CAN**) bus chip, for communication with 2 ELMO motion controllers (Gold Solo Whistle). These motor controllers receive the actual positions ($\theta_{pk}^a, \theta_{pa}^a$) and velocities ($\dot{\theta}_{pk}^a, \dot{\theta}_{pa}^a$) of the joints from an incremental encoder on the motor side of each joint and send these to the BBB along with the actual torque (τ_{pk}^a, τ_{pa}^a) of each joint. Based on these measurements, the BBB calculates the desired torques (τ_{pk}^d, τ_{pa}^d) for each joint and sends these commands to the ELMO motion controllers. The ELMO motion controllers send current to the motors.

B. EdgeDRNN Implementation

The EdgeDRNN runs on a \$90 entry-level MiniZed [34] development board. Figure 4 shows the implementation of EdgeDRNN on the MiniZed development board, which has a Zynq-7007S system-on-chip and 512 MB off-chip DDR3 memory. The Zynq-7007S has a single-core ARM Cortex-A9 CPU in the programming system (**PS**) and a programmable logic (**PL**) in the same package. EdgeDRNN is implemented on the PL with weights coming from DDR3 memory. All modules on the PL are globally driven by a 100 MHz clock.

C. System Integration

Fig. 5 shows the integrated system. The MiniZed is powered by a portable USB power bank and attached to AMPRO3 opposite the BBB. To control AMPRO3, the MiniZed takes sensor data from the BBB and sends RNN controller outputs back to the BBB. An SPI bus with BBB master interfaces the two devices. Since the BBB samples sensor data at 200 Hz, maintaining the latency of RNN

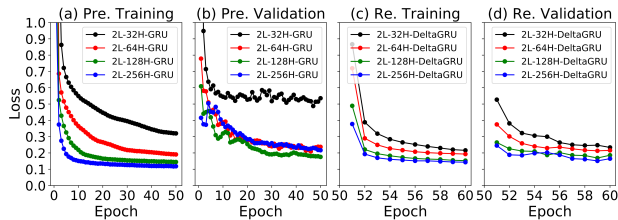


Fig. 6: Training (a) and validation (b) losses of networks in RNN pretrain (epochs 1-50) and in DeltaRNN retrain (c,d) (epochs 51-60) with $M = 32, 64, 128, 256$ and $T = 100$ time steps

TABLE I: Loss of pretrained (PRE) GRU-RNN networks and retrained (RE) DeltaGRU-RNN evaluated on the validation and test sets. Number of network parameters and the epoch where the lowest validation loss is achieved are given.

| | #Param. | Epoch | \mathcal{L} -Val. | \mathcal{L} -Test |
|---------------------|---------|-------|---------------------|---------------------|
| 2L-32H-GRU-PRE | 10 K | 47 | 0.4878 | 0.5037 |
| 2L-64H-GRU-PRE | 38 K | 46 | 0.2093 | 0.1900 |
| 2L-128H-GRU-PRE | 149 K | 50 | 0.1757 | 0.1677 |
| 2L-256H-GRU-PRE | 594 K | 50 | 0.2166 | 0.2120 |
| 2L-32H-DeltaGRU-RE | 10 K | 60 | 0.2338 | 0.2523 |
| 2L-64H-DeltaGRU-RE | 38 K | 59 | 0.2131 | 0.2207 |
| 2L-128H-DeltaGRU-RE | 149 K | 59 | 0.1690 | 0.1731 |
| 2L-256H-DeltaGRU-RE | 594 K | 59 | 0.1512 | 0.1689 |

computation under 5 ms is crucial to ensure that the control signals are received by the motors on time.

V. RESULTS AND DISCUSSION

In the following experiments, we use the RNN hardware to perform direct control on the prosthesis in place of the PD controller. This section describes the experimental set-up for the RNN controller, the evaluation methods, and results.

A. Experimental Set-up

Four different 2-layer RNN controller networks with different layer sizes $M = 32, 64, 128, 256$ were trained with a sequence length of $T = 100$ time steps, corresponding to 0.5 s of data. Each network is pre-trained on cuDNN GRU layers with a learning rate of $5e-4$ and batch size of 32 for 50 epochs. Then the cuDNN GRU parameters are loaded into DeltaGRU layers to be retrained for another 10 epochs with a learning rate of $1e-3$ and batch size of 64. We use a pretrain-retrain approach to reduce the total training time since the cuDNN GRU is highly optimized on GPUs. During retrain with a higher learning rate and larger batch size, GRU networks can be adapted to DeltaGRU networks with fewer epochs. The delta threshold Θ of DeltaGRU input and hidden activations are respectively $\Theta_x = 2^2/2^8$ and $\Theta_h = 2^7/2^8$. We used the Adam optimizer and the best network was selected according to the lowest L1 loss on the validation set. The network prediction performance in terms of L1 loss was evaluated on the test set. Training and evaluation programs are coded in PyTorch 1.2.0 with CUDA 10.1 and cuDNN 7.6. For online evaluation, the RNN controller is used for

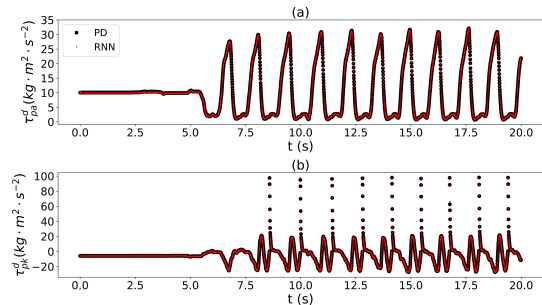


Fig. 7: Comparison of τ_{pa}^d (a) and τ_{pk}^d (b) from the PD and the RNN controller on the first 20 seconds of the test set.

a subject to walk on flat, uphill and downhill slopes (with $\approx 2.5^\circ$ slope) for 1 min tests.

B. Offline Evaluation

Figures 6(a) and (b) show the training and validation loss of the RNN controller network during epochs 1 – 50 in the pretrain stage. Training losses decrease throughout the 50 epochs. Generally larger RNN layers achieve lower validation loss but the drop rate of loss decreases with increasing layer size except that we see overfitting of the 2L-256H-GRU network on the training set; it has an even higher validation loss than 2L-128H-GRU after 50 epochs. At the beginning of the retrain stage as shown in Figs. 6(c) and (d), both training and validation losses abruptly drop due to the introduced delta threshold in DeltaGRU layers. After 10 epochs, the DeltaGRU-based networks reach similar validation losses as the corresponding GRU networks. Table I shows the results of the pretrained and retrained networks. Although the lowest test loss is achieved by the 2L-256H-DeltaGRU, we selected the 2L-128H-DeltaGRU to make the network run faster. In rest of this paper, the RNN controller refers to this network configuration.

Figure 7 shows the ankle and knee torque outputs of the RNN controller evaluated on the first 20 s of the test set. The RNN controller outputs almost overlap with the PD controller outputs indicating good cloning of the periodic behavior.

C. Online Evaluation on AMPRO3

The RNN controller network is implemented on the prosthesis in real-time, replacing the PD controller. The RNN achieves similar tracking performance as the PD controller and generalizes well to data outside of its training set.

Tracking Performance. Figure 8 shows the tracking performance (in 5 s windows) and phase portraits of the prosthetic knee joint using both controllers for 1 min of walking on flat, uphill and downhill slopes. Table II further shows the root mean square error (RMSE) between the actual and desired trajectories of the knee and the ankle joints during the 1 min online test on AMPRO3. This figure shows that both controllers perform similarly regarding stability of limit cycles though the RNN controller show slightly worse tracking performance at the beginning of each knee angle spike. The RNN controller tracking accuracy is similar to

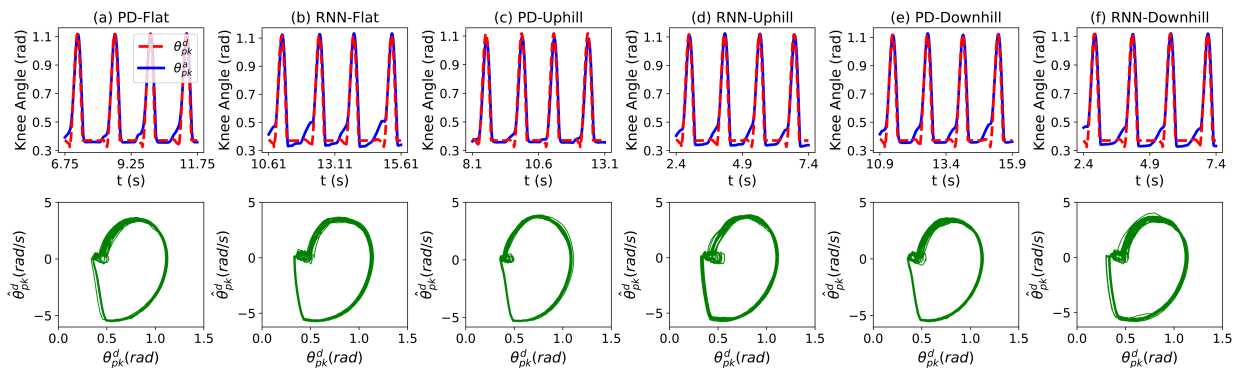


Fig. 8: Experimental tracking performance (top) and phase portrait (bottom) of the prosthetic knee joint for 1 min of walking on flat, uphill slope and downhill slope surfaces using PD and RNN controllers.

TABLE II: RMSE between actual and desired trajectories of PD and RNN controllers during a 1 min online test on AMPRO3.

| Slope | PD-Knee | RNN-Knee | PD-Ankle | RNN-Ankle |
|--------------|---------|----------|----------|-----------|
| Flat (train) | 0.0514 | 0.0592 | 0.1741 | 0.1612 |
| Uphill | 0.0437 | 0.0511 | 0.1563 | 0.1577 |
| Downhill | 0.0565 | 0.0583 | 0.1680 | 0.1708 |

TABLE III: System power breakdown (*measured by a USB power meter)

| | Power (W) |
|--|-----------|
| PS (ARM) Dynamic | 1.312 W |
| PL (EdgeDRNN) Dynamic | 0.123 W |
| On-chip Static | 0.124 W |
| Off-chip (DDR3, storage, I/O, etc.) | 0.453 W |
| MiniZed (Total)* | 2.012 W |

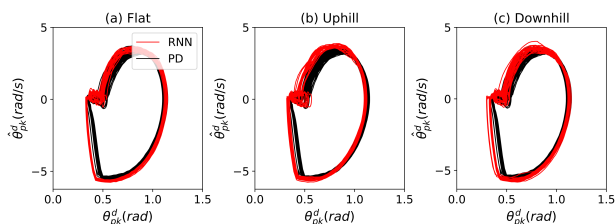


Fig. 9: Comparison between the flat-ground training set trajectories from the PD controller (identical in each plot) and trajectories from the RNN controller on different slopes during a 1 min online test on AMPRO3.

the PD controller on both knee and ankle joints for all 6 test slopes. The results show that the RNN performed similarly to the PD controller when it encountered slopes.

Generalization. To visualize the generalization ability of the RNN trained only on flat walking, Fig. 9 compares trajectories recorded during online tests of the RNN controller on flat and sloped walking with training set trajectories on flat ground. Fig. 9(a) shows that RNN and the PD trajectories on flat ground are nearly indistinguishable, which makes sense because the RNN is trained on this data. Figs. 9(b) and (c) show that the RNN maintains stable trajectories in sloped walking, which is outside the training data. This along with the results of Table II suggest the RNN generalized well.

D. Hardware Latency & Power Consumption

We measured the latency of computing the 2L-128H-DeltaGRU on EdgeDRNN using a 1 min segment of the test set that has 12,000 time steps of data. The batch size is 1, i.e. inference is run for each sample as they arrive. The average latency of each time step is $20.9 \mu\text{s}$ corresponding to 14 GOp/s throughput. By contrast the BBB has

theoretical peak throughput of 1.4 GOp/s with its 720 MHz clock. Thus EdgeDRNN achieves at least 14X higher arithmetic performance than the BBB. Table III shows the power breakdown of the MiniZed system. Whole system power is 2.012 W while the EdgeDRNN consumes only 0.123 W. Thus the EdgeDRNN system achieves 7 GOp/s/W total and 114 GOp/s/W incremental power efficiency.

VI. CONCLUSION

This paper presents the first end-to-end RNN solution for controlling a transfemoral prosthesis in a continuous action space. Experimental results show that the DeltaGRU network can be properly trained to replace the PD controller with similar tracking performance. It also maintains stable trajectories on slopes, indicating it generalized to data that is not part of its training set. With only 2 W power consumption, the EdgeDRNN accelerator on MiniZed is capable of sub-millisecond latency inference of large GRU-RNNs and realizes the prosthesis control in real-time. Future work is needed to study the stability of the RNN controller on extended test conditions (e.g. different terrains) and on different subjects. The results of this work suggest the possibility of training an RNN to learn more complex controllers that are computationally more expensive and to implement the networks on hardware accelerators for lower latency and energy consumption of the system. This hardware demonstration is a first step towards using RNNs to synergistically incorporate complex individual human gait behavior into prosthesis control, thereby closing the loop between human intent and human-prosthesis walking.

REFERENCES

- [1] T. R. Dillingham, L. E. Pezzin, and E. J. MacKenzie, "Limb amputation and limb deficiency: epidemiology and recent trends in the united states," *Southern Medical Journal*, vol. 95, no. 8, pp. 875–883, 2002.
- [2] D. Winter, *The Biomechanics and Motor Control of Human Gait: Normal, Elderly and Pathological*. University of Waterloo Press, 1991.
- [3] R. L. Waters and S. Mulroy, "The energy expenditure of normal and pathologic gait," *Gait & Posture*, vol. 9, no. 3, pp. 207–231, 1999.
- [4] E. C. Martinez-Villalpando, L. Mooney, G. Elliott, and H. Herr, "Antagonistic active knee prosthesis. a metabolic cost of walking comparison with a variable-damping prosthetic knee," in *2011 Annual International Conference of the IEEE Engineering in Medicine and Biology Society*, Aug 2011, pp. 8519–8522.
- [5] S. K. Au, J. Weber, and H. Herr, "Powered ankle-foot prosthesis improves walking metabolic economy," *IEEE Transactions on Robotics*, vol. 25, no. 1, pp. 51–66, Feb 2009.
- [6] S. Au, M. Berniker, and H. Herr, "Powered ankle-foot prosthesis to assist level-ground and stair-descent gaits," *Neural Networks*, vol. 21, no. 4, pp. 654–666, 2008, robotics and Neuroscience.
- [7] H. Zhao, J. Reher, J. Horn, V. Paredes, and A. D. Ames, "Realization of stair ascent and motion transitions on prostheses utilizing optimization-based control and intent recognition," in *Rehabilitation Robotics (ICORR), 2015 IEEE International Conference on*. IEEE, 2015, pp. 265–270.
- [8] N. Hogan, "Impedance control: An approach to manipulation," in *1984 American Control Conference*, June 1984, pp. 304–313.
- [9] F. Sup, A. Bohara, and M. Goldfarb, "Design and control of a powered transfemoral prosthesis," *The International Journal of Robotics Research*, vol. 27, no. 2, pp. 263–273, 2008, PMID: 19898683.
- [10] R. D. Gregg, T. Lenzi, L. J. Hargrove, and J. W. Sensinger, "Virtual constraint control of a powered prosthetic leg: From simulation to experiments with transfemoral amputees," *IEEE Transactions on Robotics*, vol. 30, no. 6, pp. 1455–1471, Dec 2014.
- [11] N. Aghasadeghi, H. Zhao, L. J. Hargrove, A. D. Ames, E. J. Perreault, and T. Bretl, "Learning impedance controller parameters for lower-limb prostheses," in *Intelligent robots and systems (IROS), 2013 IEEE/RSJ international conference on*. IEEE, 2013, pp. 4268–4274.
- [12] C. Cui, G. Bian, Z. Hou, X. Xie, L. Peng, and D. Zhang, "semg-based prediction of human lower extremity movements by using a dynamic recurrent neural network," in *2016 Chinese Control and Decision Conference (CCDC)*, May 2016, pp. 5021–5026.
- [13] T. Teban, R. Precup, E. Lunca, A. Albu, C. Bojan-Dragos, and E. M. Petriu, "Recurrent neural network models for myoelectricbased control of a prosthetic hand," in *2018 22nd International Conference on System Theory, Control and Computing (ICSTCC)*, Oct 2018, pp. 603–608.
- [14] K. Seo, Y. J. Park, J. Lee, S. Hyung, M. Lee, J. Kim, H. Choi, and Y. Shim, "Rnn-based on-line continuous gait phase estimation from shank-mounted imu to control ankle exoskeletons," vol. 2019, 06 2019, pp. 809–815.
- [15] S. Calinon, F. D'halluin, E. L. Sauser, D. G. Caldwell, and A. G. Billard, "Learning and reproduction of gestures by imitation," *IEEE Robotics Automation Magazine*, vol. 17, no. 2, pp. 44–54, June 2010.
- [16] Y. Pan, C.-A. Cheng, K. Saigol, K. Lee, X. Yan, E. Theodorou, and B. Boots, "Agile autonomous driving using end-to-end deep imitation learning," in *Proceedings of Robotics: Science and Systems*, Pittsburgh, Pennsylvania, June 2018.
- [17] C. Finn, T. Yu, T. Zhang, P. Abbeel, and S. Levine, "One-shot visual imitation learning via meta-learning," in *Proceedings of the 1st Annual Conference on Robot Learning*, ser. Proceedings of Machine Learning Research, S. Levine, V. Vanhoucke, and K. Goldberg, Eds., vol. 78. PMLR, 13–15 Nov 2017, pp. 357–368.
- [18] Y. Li, J. Song, and S. Ermon, "InfoGAIL: Interpretable Imitation Learning from Visual Demonstrations," in *Advances in Neural Information Processing Systems 30*, I. Guyon, U. V. Luxburg, S. Bengio, H. Wallach, R. Fergus, S. Vishwanathan, and R. Garnett, Eds. Curran Associates, Inc., 2017, pp. 3812–3822.
- [19] K. Cho, B. van Merriënboer, Ç. Gülçehre, D. Bahdanau, F. Bougares, H. Schwenk, and Y. Bengio, "Learning phrase representations using RNN Encoder–Decoder for statistical machine translation," in *Proceedings of the 2014 Conference on Empirical Methods in Natural Language Processing (EMNLP)*, Oct. 2014, pp. 1724–1734.
- [20] C. Wirth, R. Akrou, G. Neumann, and J. Fürtkranz, "A survey of preference-based reinforcement learning methods," *J. Mach. Learn. Res.*, vol. 18, no. 1, pp. 4945–4990, Jan. 2017.
- [21] H. Zhao, E. Ambrose, and A. D. Ames, "Preliminary results on energy efficient 3D prosthetic walking with a powered compliant transfemoral prosthesis," in *Robotics and Automation (ICRA), 2017 IEEE International Conference on*. IEEE, 2017, pp. 1140–1147, BestMedical Robotics Paper Award Finalist of ICRA 2017.
- [22] A. D. Ames, "Human-inspired control of bipedal walking robots," *IEEE Transactions on Automatic Control*, vol. 59, no. 5, pp. 1115–1130, 2014.
- [23] V. Azimi, T. Shu, H. Zhao, E. Ambrose, A. D. Ames, and D. Simon, "Robust control of a powered transfemoral prosthesis device with experimental verification," in *American Control Conference (ACC), 2017*. IEEE, 2017, pp. 517–522, Best Student Paper Award Finalist, ACC 2017.
- [24] S. Jiang, S. Partrick, H. Zhao, and A. D. Ames, "Outputs of human walking for bipedal robotic controller design," in *American Control Conference (ACC), 2012*. IEEE, 2012, pp. 4843–4848.
- [25] H.-H. Zhao, W.-L. Ma, M. B. Zeagler, and A. D. Ames, "Human-inspired multi-contact locomotion with AMBER2," in *Cyber-Physical Systems (ICCCPS), 2014 ACM/IEEE International Conference on*. IEEE, 2014, pp. 199–210, Best Paper Award Finalist of ICCPS 2014.
- [26] H. Zhao, J. Horn, J. Reher, V. Paredes, and A. D. Ames, "First steps toward translating robotic walking to prostheses: a nonlinear optimization based control approach," *Autonomous Robots*, vol. 41, no. 3, pp. 725–742, 2017.
- [27] B. Csaji, "Approximation with artificial neural networks," *M.S. Thesis, Dept. Science, Eotvos Lorand Univ., Budapest, Hungary*, 2001.
- [28] S. Hochreiter and J. Schmidhuber, "Long short-term memory," *Neural Comput.*, vol. 9, no. 8, pp. 1735–1780, Nov. 1997.
- [29] C. Gao, S. Braun, I. Kiselev, J. Anumula, T. Delbruck, and S. Liu, "Real-time speech recognition for iot purpose using a delta recurrent neural network accelerator," in *2019 IEEE International Symposium on Circuits and Systems (ISCAS)*, May 2019, pp. 1–5.
- [30] D. Neil, J. Lee, T. Delbrück, and S. Liu, "Delta networks for optimized recurrent network computation," in *Proceedings of the 34th International Conference on Machine Learning, ICML 2017, Sydney, NSW, Australia, 6-11 August 2017*, 2017, pp. 2584–2593.
- [31] C. Gao, D. Neil, E. Ceolini, S.-C. Liu, and T. Delbruck, "DeltaRNN: A power-efficient recurrent neural network accelerator," in *Proceedings of the 2018 ACM/SIGDA International Symposium on Field-Programmable Gate Arrays*, ser. FPGA '18. New York, NY, USA: ACM, 2018, pp. 21–30.
- [32] C. Gao, A. Rios-Navarro, X. Chen, T. Delbruck, and S.-C. Liu, "Edgedrn: Enabling low-latency recurrent neural network edge inference," 2019.
- [33] T. Osa, J. Pajarinen, G. Neumann, J. A. Bagnell, P. Abbeel, and J. Peters, *An Algorithmic Perspective on Imitation Learning*. now, 2018.
- [34] AVNET, "Minized." [Online]. Available: <http://zedboard.org/product/minized>